Experimental and computational studies on solvent-free rare-earth metal borohydrides $R(BH_4)_3$ (R=Y, Dy, and Gd)

Toyoto Sato,[1] Kazutoshi Miwa,[2,*] Yuko Nakamori,[1] Kenji Ohoyama,[1] Hai-Wen Li,[1] Tatsuo Noritake,[2] Masakazu Aoki,[2] Shin-ichi Towata,[2] and Shin-ichi Orimo[1,†]

[1]*Institute for Materials Research, Tohoku University, 2-1-1 Katahira, Aoba, Sendai 980-8577, Japan*

[2]*Toyota Central R&D Laboratories, Inc., Nagakute, Aichi 480-1192, Japan*

(Received 2 September 2007; revised manuscript received 8 February 2008; published 17 March 2008)

Solvent-free trivalent rare-earth metal borohydrides $R(BH_4)_3$ (R=Y, Dy, and Gd) were synthesized from RCl_3 and $LiBH_4$ through solid-state metathesis reactions and characterized by powder x-ray or neutron diffraction measurement and Raman spectroscopy combined with first-principles calculations. The crystal structure of $R(BH_4)_3$ was clarified to adopt a primitive cubic structure with $Y(BH_4)_3$: a=10.852(1) Å, $Dy(BH_4)_3$: a=10.885(3) Å, and $Gd(BH_4)_3$: a=10.983(5) Å in space group $Pa\bar{3}$ (No. 205), the $[BH_4]^-$ complex anions of which locate on the edges of a distorted cube composed of R^{3+}. Based on the crystal structure, the observed Raman scattering positions are theoretically assigned such that the BH_4 bending is at 1050–1300 cm^{-1} and BH_4 stretching is at 2250–2400 cm^{-1}, respectively. In addition, the computational studies on $Y(BH_4)_3$ suggested it to be an insulator that occupied B 2s,2p and H 1s orbitals with little contribution from Y, and the heat of formation was ΔH=−113 kJ/mol BH_4, which was estimated from $(1/3)Y+B+2H_2 \rightarrow (1/3)Y(BH_4)_3$.

DOI: 10.1103/PhysRevB.77.104114 PACS number(s): 61.05.fm, 61.66.Fn, 71.20.Ps, 77.22.−d

I. INTRODUCTION

Metal borohydrides $M(BH_4)_n$ [M=metal; n (valence of M)=1–4] have been attracting great interest as potential candidates for advanced hydrogen storage materials because of their high gravimetric hydrogen densities.[1–8] For this reason, the experimental and computational studies on the physical properties of $M(BH_4)_n$ have been carried out, for instance, on the stabilization mechanism governed by the charge transfer from M^{n+} to $[BH_4]^-$,[9–15] thermodynamical adjustments focusing on the Pauling electronegativity of M,[16–20] improvement of the hydrogen desorption reaction by using additives,[21–27] and so on.

In addition to the physical properties, the crystal structures have also been studied, mainly that of the monovalent borohydrides $M(BH_4)_n$ (n=1).[28–31] Typically, the hydrogen atoms are tetrahedrally coordinated around a boron atom to form $[BH_4]^-$, and the major assignments of the bending and stretching modes of $[BH_4]^-$ have been clarified to appear at around 1050–1400 and 2100–2500 cm^{-1}, respectively.[3,31,32] Furthermore, some experimental studies on the crystal structures of solvent-free multivalent borohydrides $M(BH_4)_n$ ($n \geqslant 2$) have been reported: Be,[33] Mg,[34,35] and Ca (Ref. 36) borohydrides for n=2, only Al (Ref. 37) borohydride for n=3, and Zr (Ref. 38) and Hf (Ref. 39) borohydrides for n=4.

Thus far, to the best of our knowledge, neither the crystal structures nor the physical properties of solvent-free trivalent rare-earth metal borohydrides (n=3) have been reported. In this study, therefore, trivalent rare-earth metals (R) of similar cationic sizes,[40] such as yttrium ($^{IV}Y^{3+}$=0.90 Å), dysprosium ($^{IV}Dy^{3+}$=0.91 Å), and gadolinium ($^{IV}Gd^{3+}$=0.94 Å), were selected as the metal M in $M(BH_4)_3$. In order to yield the solvent-free trivalent metal borohydrides, solid-state metathesis (SSM) reactions assisted by mechanochemical milling were employed without the use of any solutions. Subsequently, the crystal structures of $Y(BH_4)_3$ were precisely determined from a combination of high-resolution synchrotron radiation x-ray and neutron diffractions and first-principles calculations. By using the experimentally clarified crystal structure for the computational study, the physical properties of $Y(BH_4)_3$, such as B-H vibration modes, electronic property, and heat of formation, were determined by first-principles calculations. Finally, the calculated heat of formation of $Y(BH_4)_3$ was discussed in terms of the relationship with the Pauling electronegativity of yttrium.[17]

II. EXPERIMENTAL DETAILS

A. Synthesis

The starting materials, RCl_3 (99.99%; R=Y, Dy, and Gd) and $LiBH_4$ (⩾90%) powders, were purchased from Sigma-Aldrich Co. $LiBD_4$ (95.6%; Kat-Chem Ltd.) was used for the synthesis of a deuteride product for neutron diffraction measurement. The RCl_3 (R=Y, Dy, and Gd) and $LiBH_4/LiBD_4$ powders were premixed in the molar ratio of 1:3 in a mortar. The reaction was expected to proceed through SSM reaction as follows:

$$RCl_3 + 3LiBH_4/LiBD_4 \rightarrow R(BH_4)_3/R(BD_4)_3 + 3LiCl. \quad (1)$$

The mixtures were mechanochemically milled at 400 rpm in an argon atmosphere by using a Fritsch P7. To avoid temperature increase during the experiment, milling times of 15 min were alternated with 5 min of rest. The total milling time was 5 h.

B. Characterization

All the samples were investigated by an x-ray diffractometer, PANalytical X'PERT, with Cu $K\alpha$ radiation. The powder x-ray diffraction patterns were indexed by TREOR97.[41]

The suggested cell dimensions from TREOR97 were refined by the least-squares refinement program PIRUM.[42] In order to obtain high-resolution x-ray diffraction peak intensities, $Y(BH_4)_3$ was investigated at beamline BL02B2 at the Japan Synchrotron Radiation Research Institute (JASRI) SPring-8 in Hyogo, Japan. The sample was measured while rotating at room temperature for exposure times of 40 min in a large Debye–Scherrer camera of radius 286.48 mm with an image plate. The sample was loaded in a glass capillary (diameter =0.3 mm). The image was converted to a 2θ scale in the pattern range of 0.01°–75.00° in steps of $\Delta(2\theta)=0.01°$. The wavelength was calibrated to $\lambda=0.8018$ Å by using CeO_2 as the standard.

To determine the hydrogen (deuterium) atomic positions, $Y(BD_4)_3$ was investigated by neutron diffraction measurement using HERMES[43] of the Institute for Materials Research, Tohoku University, installed at the JRR-3M reactor of Japan Atomic Energy Agency, Tokai, Japan. Neutrons with a wavelength $\lambda=1.826\,46$ Å were obtained by the 331 reflection of a Ge monochromator and 12 in.-blank-sample-13 in. collimation. The fine powder sample was sealed in a helium-gas-filled cylindrical vanadium sample holder (diameter=3 mm) and mounted at the cold head of a closed cycle helium-gas refrigerator. The neutron diffraction pattern was collected from $2\theta=7°-157°$ in steps of $\Delta(2\theta)=0.1°$ at 17 K for 24 h.

Determinations of the atomic positions from the synchrotron x-ray and neutron powder diffraction patterns were combined with the *ab initio* structural determination program FOX (Ref. 44) and the Rietveld program FULLPROF (Ref. 45) in the pattern range $2\theta=5.0°-40°$ and 7°–120°, respectively. Two modified Lorentzian and Gaussian peak shape functions were used for the Rietveld program for the x-ray and neutron diffraction patterns, respectively.

The Raman spectra of all the products were obtained by using a Nicolet Almega-HD with a $Nd:YVO_4$ laser (532 nm). The products were placed and observed in an argon-gas-filled sample holder with a glass window.

III. COMPUTATIONAL DETAILS

The presented calculations were performed using the ultrasoft pseudopotential method[46] based on density functional theory.[47] The generalized gradient approximation[48] (GGA) was adopted for the exchange-correlation energy. For Y, the $4s$ and $4p$ semicore states were treated as valence. During the structural optimizations, the cutoff energies were set at 15 and 180 hartrees for the pseudowave functions and the charge density, respectively, and k-point sampling was performed using a $2\times2\times2$ special-point grid.[49] The optimization procedure was continued until the residual force and stress became less than 1×10^{-3} hartree/bohr and 0.1 GPa, respectively. When the optimized structure was obtained, the total energy was recalculated with a denser $4\times4\times4$ k-point grid including the Γ point.

IV. RESULTS AND DISCUSSION

A. Preliminary experimental analyses of $R(BH_4)_3$

All the samples were investigated using an x-ray diffractometer (Fig. 1). They exhibited similar diffraction patterns

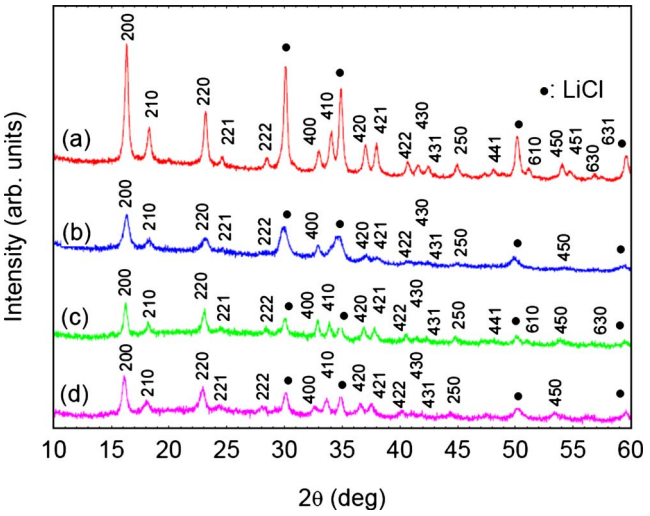

FIG. 1. (Color online) X-ray diffraction patterns of $R(BH_4)_3$ [R=(a) Y, (b) Y (deuteride), (c) Dy, and (d) Gd].

with a LiCl phase and unknown peaks. The diffraction peaks from $LiBH_4/LiBD_4$ and R chlorides, hydrides or deuterides, borides, and oxides were not identified in all the patterns. Assuming that the unknown peaks belong to a single phase, a primitive cubic unit cell could be indexed. The indices are indicated on the patterns in Fig. 1. The space group could be described as space group $Pa\bar{3}$ (No. 205) from the reflection conditions. The lattice parameters are listed in Table I. The contraction of the lattice parameters could follow the lanthanoid contraction.

All the samples were also observed by Raman spectroscopy (Fig. 2). None of the scatterings agreed with those of the starting materials, RCl_3 and $LiBH_4/LiBD_4$. Although they did not belong to $LiBH_4/LiBD_4$, the Raman scatterings could be assigned to the B-H/B-D bending and stretching vibration modes when compared with those of $LiBH_4/LiBD_4$ (black dashed lines in each spectrum in Fig. 2).[3,31,32] The bending modes at around 1145 and 1340 cm^{-1} were clearly distinguished from those of $LiBH_4$. The sloped baseline of $Gd(BH_4)_3$ [Fig. 2(d)] at high frequency causes the fluorescence from Gd $4f$ orbital.

From both of the x-ray diffraction and Raman spectroscopic results, it was confirmed that $R(BH_4)_3$ could be derived from the SSM reaction [Eq. (1)].

TABLE I. Lattice parameters a of $R(BH_4)_3$.

$R(BH_4)_3$	a (Å)
$Y(BH_4)_3$[a]	10.852(1)
$Y(BD_4)_3$[b]	10.843(5)
$Dy(BH_4)_3$[c]	10.885(3)
$Gd(BH_4)_3$[d]	10.983(5)

[a]Figure 1(a).
[b]Figure 1(b).
[c]Figure 1(c).
[d]Figure 1(d).

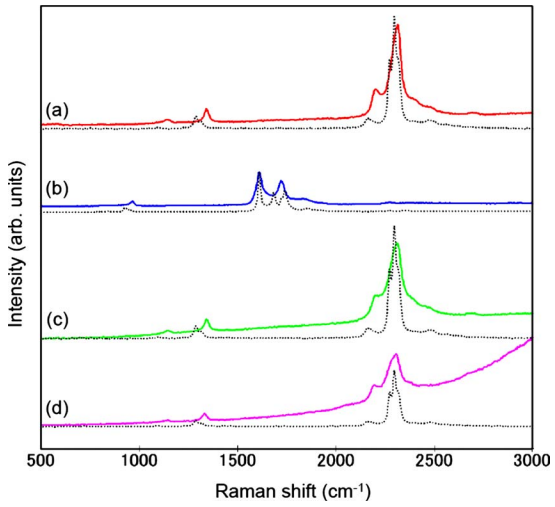

FIG. 2. (Color online) Raman spectra of $R(BH_4)_3$ [R=(a) Y, (b) Y (deuteride), (c) Dy, and (d) Gd]. Black dashed lines are $LiBH_4$ and $LiBD_4$ as references on each Raman spectrum.

B. Crystal structure of $Y(BH_4)_3$ and $Y(BD_4)_3$

To determine the crystal structure of $R(BH_4)_3$, $Y(BH_4)_3$ was used because it exhibited the best crystallinity among all the samples (cf. Fig. 1). At first, the Y and B atomic positions were determined from high-resolution synchrotron radiation x-ray diffraction. The atoms in space group $Pa\bar{3}$ with a =10.852(1) Å and the synchrotron data were the input for the *ab initio* structural determination program FOX.[44] According to the FOX result, the Y and B atoms were at (0.218 041, 0.211 943, 0.218 871) and (0.194 784, 0.238 961, 0.968 635), which could be at the 8*c* and 24*d* sites, respectively. The Y:B atomic ratio, therefore, corresponds to the stoichiometric composition of $Y(BH_4)_3$. By using the FOX result, the Rietveld program FULLPROF (Ref. 45) was carried out. The calculated Rietveld profile was in good agreement with the observed peak intensities (R_B=6.38% and R_F =3.67%).

Next, the hydrogen atomic positions were determined by using the neutron diffraction pattern of $Y(BD_4)_3$. (Commercial $LiBD_4$ with natural boron was used as the starting material.) The neutron diffraction was measured at 17 K in order to restrain the temperature factor of deuterium (D). The initial atomic positions of $Y(BD_4)_3$ were predicted from first-principles calculations (the details are described in Sec. IV C).[50] By using the predicted structure, the refinement result of the neutron diffraction pattern was obtained. It provided a reasonably good fit in the refinement (Fig. 3) (R_B =12.4% and R_F=9.20%). The crystallographic parameters are listed in Table II. The B and D atomic positions could not be finally refined. The reason for this could be the high-neutron-absorption cross-section element of B (767 barn).[51] Thus, the initial predicted B and D positions were used, maintaining the B-D distances for the refinement.

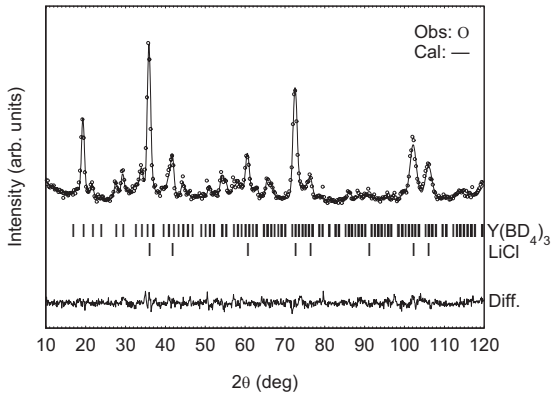

FIG. 3. Rietveld profile refinement with neutron diffraction data (○) of $Y(BD_4)_3$ in space group $Pa\bar{3}$ (No. 205). Reflection makers are for $Y(BD_4)_3$ and LiCl from above.

The crystal structure is illustrated in Fig. 4. The $[BD_4]^-$ complex anions are located on the edges of a distorted Y^{3+} cation cube. Y^{3+} is surrounded by six $[BD_4]^-$. The arrangement of Y^{3+} and $[BD_4]^-$ is basically a distorted ReO_3-type substructure (yellow dashed line in Fig. 4) within the structure of $Y(BD_4)_3$.

From the results in Secs. IV A and IV B, it can be concluded that $R(BH_4)_3$ adopts the same crystal structure as that of $Y(BH_4)_3$. [In Appendix A, a structure map and a table with the unit cell parameters of metal borohydrides $M(BH_4)_n$ (n=1–4) are added to systematically understand their crystal structure.]

C. First-principles studies of $Y(BH_4)_3$

By using the refinement results of the synchrotron radiation data, first-principles calculations were performed.[50] The Y-B-Y angle has 170.2°, with B-Y distances of 2.71 and 2.79 Å. Since Y-B-Y has been found to be nearly linear with almost equal B-Y interatomic distances, it is naturally expected that the tetrahedral $[BH_4]^-$ complex is arranged so as to form two edge (μ_2) bonds with two Y atoms, that is,

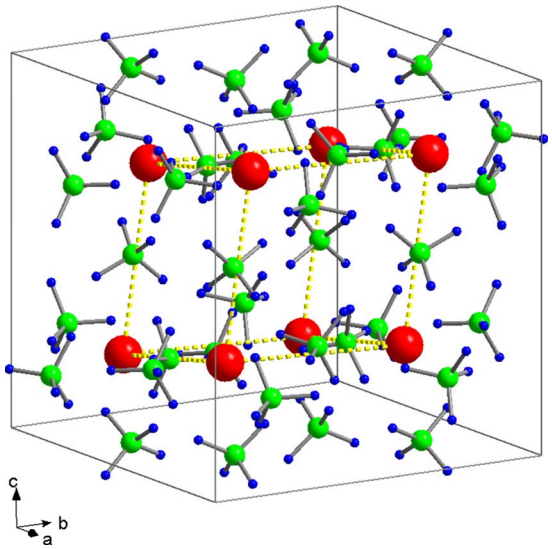

FIG. 4. (Color online) Crystal structure of $Y(BD_4)_3$ [Y (red), B (green), and D (blue)]. Complex anion $[BD_4]^-$ locate on the edges of the distorted cube of cation Y^{3+} (yellow dashed line).

TABLE II. Crystallographic parameters for $Y(BD_4)_3$ with $a=10.771(4)$ Å at 17 K [$a=10.894$ Å (predicted)] in space group $Pa\bar{3}$ (No. 205) and $Z=8$. The predicted values are given in parentheses. (B and D positions and temperature factor of B are not refined).

Atom	Site	x	y	z	B_{iso}	Occupancy
Y	8*c*	0.211(1) (0.2165)	0.211(1) (0.2165)	0.211(1) (0.2165)	0.6(6)	1.00 (1.00)
B	24*d*	0.19200 (0.19200)	0.24750 (0.24750)	0.96710 (0.96710)	1.0	1.00 1.00
D1 (H1)	24*d*	0.29000 (0.29000)	0.25400 (0.25400)	0.02410 (0.02410)	2.2(2)	1.00 (1.00)
D2 (H2)	24*d*	0.10300 (0.10300)	0.22450 (0.22450)	0.03400 (0.03400)	2.2(2)	1.00 (1.00)
D3 (H3)	24*d*	0.17370 (0.17370)	0.34810 (0.34810)	0.91810 (0.91810)	2.2(2)	1.00 (1.00)
D4 (H4)	24*d*	0.20180 (0.20180)	0.16260 (0.16260)	0.89230 (0.89230)	2.2(2)	1.00 (1.00)

$Y(\mu_2\text{-}H_2BH_2\text{-}\mu_2)Y$. Assuming that the hydrogen atoms satisfy the $Pa\bar{3}$ symmetry, structural optimization was performed using four different initial configurations. For the first configuration, four hydrogen atoms, which were used as seeds to generate all the hydrogen positions in the unit cell, were placed at $(\pm 0.816d, 0, 0.577d)$ and $(0, \pm 0.816d, -0.577d)$ around a B atom occupying the center of a cube edge parallel to the c axis, where $d=1.23$ Å. The other three initial configurations were generated by rotating the four seed atoms about the c axis by 45°, 90°, and 135°, respectively.

The values in parentheses in Table II show the crystallographic parameters for the most stable geometry obtained in our structural optimization process. The lattice parameter and atomic positions for Y and B are in good agreement with the experimental data. The B-H bond lengths and the H-B-H angles were predicted to be 1.24 Å and 107°–113°, respectively. The buckling of $Y(\mu_2\text{-}H_2BH_2\text{-}\mu_2)Y$ chains is visible in Fig. 4.

The Γ-phonon frequencies were calculated (Fig. 5), where the contribution of only the transverse-optical mode was taken into consideration. These eigenmode frequencies can be classified into three groups. By analyzing the eigenvectors, we confirmed that the eigenmodes in the regions 1050–1300 and 2250–2400 cm^{-1} originated from the internal B-H bending and stretching vibrations of the $[BH_4]^-$ complex, respectively. These frequencies are in fairly good agreement with those obtained using the molecular approximation for a free $[BH_4]^-$ complex.[9] The eigenmodes with low frequencies (<600 cm^{-1}) include librational ones, which involve nearly rigid displacements of the $[BH_4]^-$ complex. The computational results were found to be close to the observed Raman

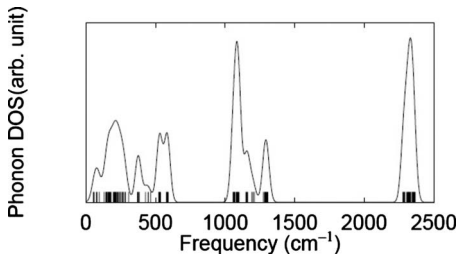

FIG. 5. Phonon density of states for $Y(BH_4)_3$. The contribution of Γ-phonon transverse-optical modes indicated by vertical bars is only taken into account and the Gaussian broadening with a width of 30 cm^{-1} is used.

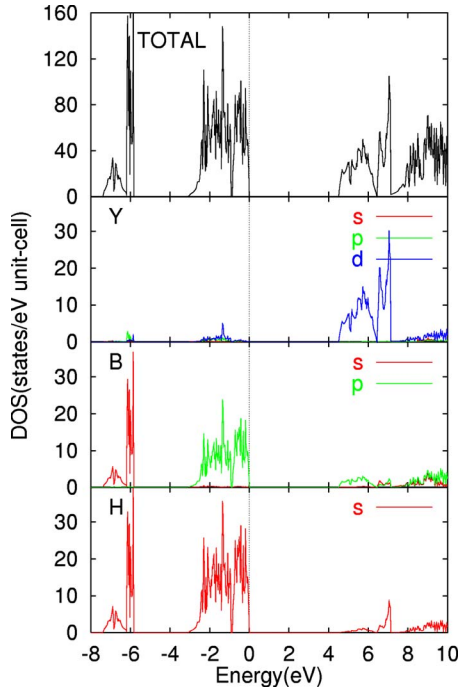

FIG. 6. (Color online) Total and partial densities of states for $Y(BH_4)_3$. The origin of energy is set to be the top of valence states.

TABLE III. Cohesive energies E_{coh} (eV/atom) and zero-point energies E_{ZPE} (eV/atom) for $Y(BH_4)_3$ and related elements. Note that the zero-point energies are not included in E_{coh}.

	E_{coh}	E_{ZEP}
$Y(BH_4)_3$	−3.455	0.200
Y	−4.703	0.025
B[a]	−6.201	0.126
H_2[a]	−2.272	0.135

[a]The values are obtained from Ref. 9.

scatterings at 590, 1145, 1340, 2200, 2310, 2390, and 2460 cm^{-1}.

The total and partial densities of states for $Y(BH_4)_3$ are shown in Fig. 6. The electronic structure is nonmetallic with a calculated energy gap of 4.5 eV. The occupied states mainly consist of B $2s,2p$ and H $1s$ orbitals and there is little contribution from Y orbitals. This supports an ionic picture for the interaction between metal atoms and $[BH_4]^-$ complexes.[9,17,36]

Finally, the heat of formation can be calculated from the crystal structure. The cohesive energies and zero-point energies (ZPEs) for $Y(BH_4)_3$ and related compounds are summarized in Table III. For $Y(BH_4)_3$, the ZPE is evaluated from only the transverse-optical Γ eigenmode frequencies, namely, we neglect the effect of the dipole-dipole interaction.[9] We can expect that the error caused by this treatment is negligibly small. For example, this approximation introduces only a change of 0.4 kJ/mol in the heat of formation of $Ca(BH_4)_2$. For hcp-Y, the lattice parameters are predicted to be $a=3.642$ Å and $c=5.680$ Å, which agreed well with the experimental values ($a=3.65$ and $c=5.73$ Å), and the ZPE is calculated using a supercell containing 36 atmos. From Table III, the heat of formation for the reaction

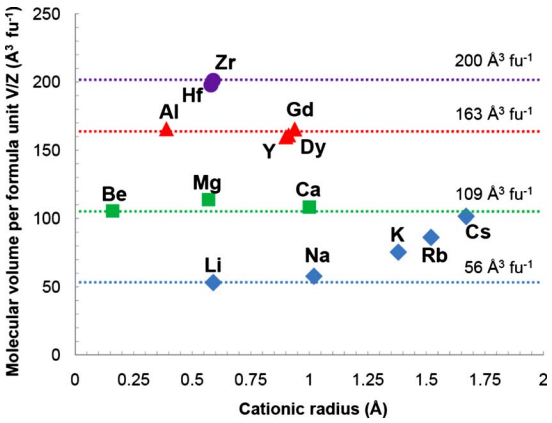

FIG. 7. (Color online) Structure map for metal borohydrides $M(BH_4)_n$ with respect to molecular volume per formula unit and cationic radius classified by charge valence of M^{n+} (blue, monovalence; green, divalence; red, trivalence; and purple, tetravalence). Dashed lines and values indicate the average volume per formula unit for each charge valence of M^{n+}.

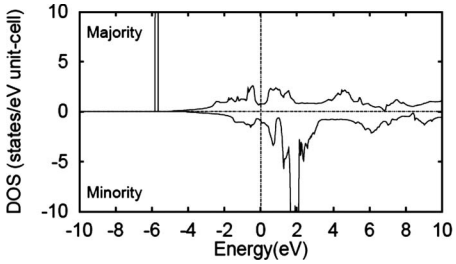

FIG. 8. Electronic density of states for hcp-Gd. The origin of energy is set to be the Fermi level.

$$(1/3)Y + B + 2H_2 \rightarrow (1/3)Y(BH_4)_3 \quad (2)$$

is predicted to be $\Delta H=-113(-151)$ kJ/mol BH_4 with (without) the ZPE correction, where the heat of formation is normalized by the number of BH_4 complexes in formula unit for comparison purposes.[17] For metal borohydrides, a correlation has been reported between the normalized heats of formation ΔH and the Pauling electronegativities of M, χ_P.[17,19,36] This correlation can be represented approximately by the following linear relationship[17,19]:

$$\Delta H = 253.6\chi_P - 398.0. \quad (3)$$

Since $\chi_P=1.2$ for Y, Eq. (3) affords $\Delta H=-94$ kJ/mol BH_4. The agreement between this estimated value and the predicted one is reasonably good. The theoretical prediction of the thermodynamical stability for $Gd(BH_4)_3$ is described in Appendix B.

V. SUMMARY

The solvent-free rare-earth metal borohydrides $R(BH_4)_3$ (R=Y, Dy, and Gd) were synthesized from RCl_3 and $LiBH_4$ by the SSM reaction.

$R(BH_4)_3$ were then experimentally characterized by powder x-ray or neutron diffraction and Raman spectroscopy as follows: (i) The crystal structure was clarified to adopt a cubic structure with $Y(BH_4)_3$: $a=10.852(1)$ Å, $Dy(BH_4)_3$: $a=10.885(3)$ Å, and $Gd(BH_4)_3$: $a=10.983(5)$ Å in space group $Pa\bar{3}$ (No. 205), in which $[BH_4]^-$ complex anions locate on the edges of a distorted cube composed of R^{3+}.

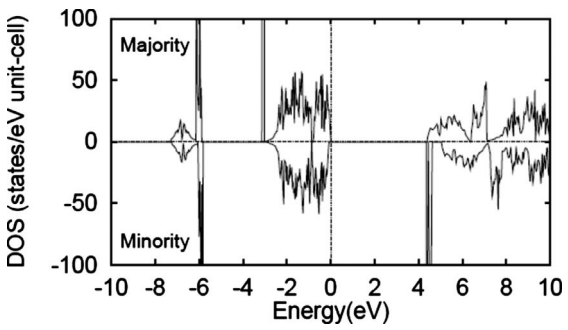

FIG. 9. Electronic density of states for $Gd(BH_4)_3$. The origin of energy is set to be the top of valence states.

TABLE IV. Modifications of $M(BH_4)_n$.

$M(BH_4)_n$	Crystal system	Lattice parameter (Å)	Volume (Å^3)	Z	V/Z (Å^3/f.u.)	Ref.
$LiBH_4$	Orthorhombic (LT)[a]	a=7.3635 b=4.3982 c=6.5965	213.64	4	53.41	28
	Hexagonal (HT)	a=4.1956 c=6.6013	100.63	2	50.32	
$NaBH_4$	Tetragonal (LT)	a=4.332 c=5.869	110.14	2	55.07	30
	Cubic (HT)[a]	a=6.137	231.14	4	57.79	
KBH_4	Tetragonal (LT)	a=4.6836 c=6.5707	114.14	2	57.07	31
	Cubic (HT)[a]	a=6.7074	301.76	4	75.44	
$RbBH_4$	Cubic (LT)	a=6.9039	329.07	4	82.27	31
	Cubic (HT)[a]	a=7.0156	345.30	4	86.33	
$CsBH_4$	Cubic (LT)	a=7.2898	387.39	4	96.85	31
	Cubic (HT)[a]	a=7.4061	406.23	4	101.56	
$Be(BH_4)_2$	Tetragonal	a=13.62 c=9.10	1688.09	16	105.51	33
$Mg(BH_4)_2$	Hexagonal (LT)[a]	a=10.3414 c=37.086	3434.7	30	114.49	34 and 35
	Orthorhombic (HT)	a=37.072 b=18.6476 c=10.9123	7543.8	64	117.87	
$Ca(BH_4)_2$	Orthorhombic	a=8.791 b=13.137 c=7.500	866.16	8	108.27	36
$Al(BH_4)_3$	Monoclinic (LT)[a]	a=21.914 b=5.986 c=21.787 β=111.90°	2652.1	16	165.76	37
	Orthorhombic (HT)	a=18.021 b=6.138 c=6.1987	17.43	4	171.43	
$Y(BH_4)_3$	Cubic	a=10.852	1278.00	8	159.75	This work
$Dy(BH_4)_3$	Cubic	a=10.885	1289.69	8	161.21	This work
$Gd(BH_4)_3$	Cubic	a=10.983	1324.84	8	165.61	This work
$Zr(BH_4)_4$	Cubic	a=5.86	201.23	1	201.23	38
$Hf(BH_4)_4$	Cubic	a=5.827	197.85	1	197.85	39

[a]These phase values are used for Fig. 7.

(ii) BH_4 bonding modes of $R(BH_4)_3$, which were guessed compared with vibration modes of $LiBH_4$, appear at 590, 1145, 1340, 2200, 2310, 2390, and 2460 cm^{-1}.

Based on the experimental characterization above, the physical properties of $Y(BH_4)_3$ were computationally studied as follows: (i) Phonon calculation assigned the experimentally observed Raman scatterings of $Y(BH_4)_3$ such that 1145 and 1340 cm^{-1} indicate the BH_4 bending mode, and 2200, 2390, and 2460 cm^{-1} indicate the BH_4 stretching modes, respectively. The Raman scattering at 590 cm^{-1} caused the dis-

placement of $[BH_4]^-$. (ii) Electronic property and the heat of formation were also calculated. $Y(BH_4)_3$ was found to be an insulator with an energy gap of 4.5 eV, where B $2s,2p$ and H $1s$ orbitals were occupied, with little contribution from Y. The heat of formation for $Y(BH_4)_3$ was $\Delta H=-113$ kJ/mol BH_4, which obeyed a correlation of $M(BH_4)_n$ between the heat of formation and the Pauling electronegativity of M.

Based on their structural characterizations, further studies on the physical properties of the other solvent-free multivalent borohydrides $M(BH_4)_n$ ($n \geqslant 2$) are now being investigated.

ACKNOWLEDGMENTS

This work was partially supported by KAKENHI (18206073), by Global COE Program (B03, Tohoku University), and by the New Energy and Industrial Technology Development Organization (NEDO), "Development for Safe Utilization and Infrastructure of hydrogen" Project. The synchrotron radiation experiment was performed at SPring-8 as No. 2006B0127 which was approved by the Japan Synchrotron Radiation Research Institute (JASRI).

APPENDIX A

Figure 7 shows the molecular volume per formula unit V/Z vs cation radius of M (V the volume of crystal structure and Z the number of molecules in a unit cell) for borohydrides $M(BH_4)_n$ ($n=1-4$). The unit cell parameters of the crystal structure of $M(BH_4)_n$ are listed in Table IV. The V/Z becomes higher with a higher charge valence of M because the $M(BH_4)_n$ has more $[BH_4]^-$ units in the crystal structure. The volume per valence n of M is, however, approximately the same ($\approx 50-55$ Å^3/f.u.), except for monovalent borohydrides $M(BH_4)_n$. [In all the cases, the volume per valence n of M conspicuously shows dependence on cation size. It could be due to the cation size effect because $NaBH_4$, KBH_4, $RbBH_4$, and $CsBH_4$ have the same atomic arrangements with large cations radius difference ($^{VI}Na^+$: 1.02 Å, $^{VI}K^+$: 1.38 Å, $^{VI}Rb^+$: 1.52 Å, and $^{VI}Cs^+$: 1.67 Å)].

Figure 7 is also useful for structural modeling. The figure can help determine a suitable unit cell and the number of atoms (or molecules) in a unit cell for $M(BH_4)_n$. By using the suggestions, the Pearson symbol or the structure type can be determined.

APPENDIX B

Since the Pauling electronegativities for Gd and Dy are close to that of Y,[52] we can expect that the thermodynamical stabilities of $Gd(BH_4)_3$ and $Dy(BH_4)_3$ are also similar to that of $Y(BH_4)_3$. In the rare-earth compounds, the strong on-site f-f interactions play the important role of pushing the $4f$ electrons toward localization. The conventional density functional theory (DFT) calculation as performed in this study is insufficient to account for this strong correlation, particularly for an open f-shell system, and more sophisticated approaches are usually required.[53–55] Fortunately, neutral Gd as well as Gd^{3+} has a half-filled $4f$ shell and so it is expected that most of the drawbacks of the DFT calculation are hidden for the Gd system. In this appendix, we show the result of the DFT calculation for $Gd(BH_4)_3$.

TABLE V. Predicted crystallographic parameters for $Gd(BH_4)_3$ with $a=11.008$ Å in space group $Pa\bar{3}$ (No. 205) and $Z=8$.

Atom	Site	x	y	z
Gd	8c	0.2169	0.2169	0.2169
B	24d	0.1919	0.2475	0.9670
H1	24d	0.2892	0.2539	0.0231
H2	24d	0.1039	0.2248	0.0335
H3	24d	0.1736	0.3472	0.9186
H4	24d	0.2012	0.1633	0.8931

For the Gd pseudopotential, the semicore $5s$ and $5p$ states are treated as valence states. Because of the highly localized nature of Gd $4f$ orbitals, the cutoff energies are set to be 25 and 200 hartrees for the pseudowave functions and the charge density, respectively. For the Gd metal, which is a ferromagnet with the hcp structure in the ground state, the lattice parameters are obtained as $a=3.646$ Å and $c=5.842$ Å. These predicted values are in good agreement with the experimental ones ($a=3.63$ Å and $c=5.78$ Å). Figure 8 depicts the electronic density of states (DOS) for hcp-Gd. The fully occupied $4f^{\uparrow}$ states located at about -6 eV form a sharp peak, whereas the unoccupied $4f^{\downarrow}$ states at around 2 eV show some dispersion. These characteristics resemble those obtained using the quasiparticle self-consistent GW calculation,[55] though our DFT calculation with GGA underestimates the exchange splitting between filled $4f^{\uparrow}$ and empty $4f^{\downarrow}$ levels.

For $Gd(BH_4)_3$, the structural optimization is performed starting from the optimized configuration for $Y(BH_4)_3$, where the ferromagnetic structure is assumed. The lattice parameter is predicted to be $a=11.008$ Å, which is slightly larger than that of $Y(BH_4)_3$ as observed experimentally. Table V summarizes the optimized crystallographic parameters for $Gd(BH_4)_3$, which are quite similar to those of $Y(BH_4)_3$. Figure 9 indicates the electronic DOS for $Gd(BH_4)_3$. The electronic structure is nonmetallic, in which the filled Gd $4f^{\uparrow}$ and empty $4f^{\downarrow}$ states are found at -3 and 4.5 eV, respectively. The normalized heat of formation for $Gd(BH_4)_3$, corresponding to the reaction of Eq. (2), is obtained as $\Delta H=-148$ kJ/mol BH_4 without the ZPE correction.[56] As expected, this value is very close to that of $Y(BH_4)_3$ (-151 kJ/mol BH_4).

*miwa@cmp.tytlabs.co.jp
†orimo@imr.tohoku.ac.jp

[1] A. Züttel, P. Wenger, S. Rentsch, P. Sudan, Ph. Mauron, and Ch. Emmenegger, J. Power Sources **118**, 1 (2003).
[2] A. Züttel, P. Fisher, P. Sudan, Ph. Mauron, and S. Orimo, Mater. Sci. Eng., B **108**, 9 (2004).
[3] S. Orimo, Y. Nakamori, and A. Züttel, Mater. Sci. Eng., B **108**, 51 (2004).
[4] S. Orimo, Y. Nakamori, G. Kitahara, K. Miwa, N. Ohba, S. Towata, and A. Züttel, J. Alloys Compd. **404-406**, 427 (2005).
[5] S. Orimo, Y. Nakamori, N. Ohba, K. Miwa, M. Aoki, S. Towata, and A. Züttel, Appl. Phys. Lett. **89**, 021920 (2006).
[6] M. Dornheim, N. Eigen, G. Barkhordarian, T. Klassen, and R. Bormann, Adv. Eng. Mater. **8**, 377 (2006).
[7] K. Chlopek, C. Frommen, A. Léon, O. Zabala, and M. Fichtner, J. Mater. Chem. **17**, 3465 (2007).
[8] S. Orimo, Y. Nakamori, J. R. Eliseo, A. Züttel, and C. M. Jensen, Chem. Rev. (Washington, D.C.) **107**, 4111 (2007).
[9] K. Miwa, N. Ohba, S. I. Towata, Y. Nakamori, and S. I. Orimo, Phys. Rev. B **69**, 245120 (2004).
[10] Q. Ge, J. Phys. Chem. A **108**, 8682 (2004).
[11] T. J. Frankcombe, G.-J. Kroes, and A. Züttel, Chem. Phys. Lett. **405**, 73 (2005).
[12] N. A. Zarkevich and D. D. Johnson, Phys. Rev. Lett. **97**, 119601 (2006).
[13] Z. Łodziana and T. Vegge, Phys. Rev. Lett. **97**, 119602 (2006).
[14] T. J. Frankcombe and G.-J. Kroes, Phys. Rev. B **73**, 174302 (2006).
[15] H.-W. Li, K. Kikuchi, Y. Nakamori, N. Ohba, K. Miwa, S. Towata, and S. Orimo, Acta Mater. **56**, 1342 (2008).
[16] K. Miwa, N. Ohba, S. Towata, Y. Nakamori, and S. Orimo, J. Alloys Compd. **404-406**, 140 (2005).
[17] Y. Nakamori, K. Miwa, A. Ninomiya, H.-W. Li, N. Ohba, S. Towata, A. Züttel, and S. Orimo, Phys. Rev. B **74**, 045126 (2006).
[18] Y. Nakamori, H.-W. Li, K. Kikuchi, M. Aoki, K. Miwa, S. Towata, and S. Orimo, J. Alloys Compd. **446-447**, 296 (2007).
[19] K. Miwa, N. Ohba, S. Towata, Y. Nakamori, A. Züttel, and S. Orimo, J. Alloys Compd. **446-447**, 310 (2007).
[20] H.-W. Li, S. Orimo, Y. Nakamori, K. Miwa, N. Ohba, S. Towata and A. Züttel, J. Alloys Compd. **446-447**, 315 (2007).
[21] J. J. Vajo, S. L. Skeith, and F. Mertens, J. Phys. Chem. B **109**, 3719 (2005).
[22] M. Au and A. Jurgensen, J. Phys. Chem. B **110**, 7062 (2006).
[23] M. Au, A. Jurgensen, and K. Zeigler, J. Phys. Chem. **110**, 26482 (2006).
[24] X. B. Yu, Z. Wu, Q. R. Chen, Z. L. Li, B. C. Weng, and T. S. Huang, Appl. Phys. Lett. **90**, 034106 (2006).
[25] X. B. Yu, D. M. Grant, and G. S. Walker, Chem. Commun. (Cambridge) **2006**, 3906.
[26] J. J. Vajo and G. L. Olson, Scr. Mater. **56**, 829 (2007).
[27] H.-W. Li, K. Kikuchi, Y. Nakamori, K. Miwa, S. Towata, and S. Orimo, Scr. Mater. **57**, 679 (2007).
[28] P. Vajeeston, P. Ravindran, A. Kjekshus, and H. Fjellvåg, J. Alloys Compd. **387**, 97 (2005).
[29] R. L. Davis and C. H. L. Kennard, J. Solid State Chem. **59**, 393 (1985).
[30] P. Fischer and A. Züttel, Mater. Sci. Forum **443-444**, 287 (2004).
[31] G. Renaudin, S. Gomes, H. Hagemann, L. Keller, and K. Yvon, J. Alloys Compd. **375**, 98 (2004).
[32] Y. Nakamori and S. Orimo, J. Alloys Compd. **370**, 271 (2004).
[33] D. S. Marynick and W. N. Lipscomb, Inorg. Chem. **11**, 820 (1972).
[34] R. Černý, Y. Filinchuk, H. Hagemann, and K. Yvon, Angew. Chem., Int. Ed. **46**, 1 (2007).
[35] J.-H. Her, P. W. Stephens, Y. Gao, G. L. Solveichik, J. Riijssenbeek, M. Andrus, and J.-C. Zhao, Acta Crystallogr., Sect. B: Struct. Sci. **B63**, 561 (2007).
[36] K. Miwa, M. Aoki, T. Noritake, N. Ohba, Y. Nakamori, S. I. Towata, A. Züttel, and S. I. Orimo, Phys. Rev. B **74**, 155122 (2006).
[37] S. Aldridge, A. J. Blake, A. J. Downs, R. O. Gould, S. Parsons, and C. R. Pulham, J. Chem. Soc. Dalton Trans. **1997**, 1007.
[38] P. H. Bird and M. R. Churchill, Chem. Commun. (London) **8**, 403 (1967).
[39] R. W. Broach, I.-S. Chuang, T. J. Marks, and J. M. Williams, Inorg. Chem. **22**, 1081 (1983).
[40] http://abulafia.mt.ic.ac.uk/shannon/ptable.php
[41] P.-E. Werner, L. Eriksson, and M. Westdahl, J. Appl. Crystallogr. **18**, 367 (1985).
[42] P.-E. Werner, Ark. Kemi **31**, 513 (1969).
[43] K. Ohoyama, T. Kanouchi, K. Nemoto, M. Ohashi, T. Kajitani, and Y. Yamaguchi, Jpn. J. Appl. Phys., Part 1 **37**, 3319 (1998).
[44] V. Favre-Nicolin and R. Černý, J. Appl. Crystallogr. **35**, 734 (2002); http://objcryst.sourceforge.net
[45] J. Rodriguez-Carvajal, FULLPROF, Version 3.2, March 2005.
[46] D. Vanderbilt, Phys. Rev. B **41**, 7892 (1990); L. Laasonen, A. Pasquarello, R. Car, C. Lee, and D. Varderbilt, *ibid.* **47**, 10142 (1993).
[47] P. Hohenberg and W. Kohn, Phys. Rev. **136**, B864 (1964); W. Kohn and L. J. Sham, *ibid.* **140**, A1133 (1965).
[48] J. P. Perdew, K. Burke, and M. Ernzerhof, Phys. Rev. Lett. **77**, 3865 (1996); **78**, 1396(E) (1997).
[49] H. J. Monkhorst and J. D. Pack, Phys. Rev. B **13**, 5188 (1976).
[50] The structural determination procedures were as follows: At first, Y and B atomic positions in $Y(BH_4)_3$ were determined from synchrotron radiation data. Next, H atomic positions in $Y(BH_4)_3$ were predicted from first-principles calculations by using the synchrotron result as the initial structural modeling. Finally, the crystal structure of $Y(BD_4)_3$ was determined from neutron diffraction data, where the computational result was used as the initial atomic positions.
[51] http://www.ncnr.nist.gov/resources/n-lengths/
[52] The Pauling electronegativities revised by Allred are 1.22, 1.20, and 1.22 for Y, Gd, and Dy, respectively [A. L. Allred, J. Inorg. Nucl. Chem. **17**, 215 (1961)].
[53] S. Fabris, S. deGironcoli, S. Baroni, G. Vicario, and G. Balducci, Phys. Rev. B **71**, 041102(R) (2005).
[54] L. Petit, A. Svane, Z. Szotek, and W. M. Temmerman, Phys. Rev. B **72**, 205118 (2005).
[55] A. N. Chantis, M. van Schilfgaarde, and T. Kotani, Phys. Rev. B **76**, 165126 (2007).
[56] The binding energies for B and H_2 are recalculated using the higher cutoff energy (25 and 200 hartrees), although this treatment raises ΔH by 1 kJ/mol BH_4 only.